Biochimica et Biophysica Acta 1844 (2014) 422–429

Contents lists available at ScienceDirect

Biochimica et Biophysica Acta

journal homepage: www.elsevier.com/locate/bbapap

Crystal structure and biochemical characterization of a manganese superoxide dismutase from *Chaetomium thermophilum*

Teemu Haikarainen [a,b,1], Clémence Frioux [a,b], Li-Qing Zhnag [c,d], Duo-Chuan Li [c], Anastassios C. Papageorgiou [a,b,*]

[a] Turku Centre for Biotechnology, University of Turku, BioCity, Turku 20521, Finland
[b] Åbo Akademi University, BioCity, Turku 20521, Finland
[c] Department of Environmental Biology, Shandong Agricultural University, Taian, Shandong 271018, China
[d] Department of Chemistry and Chemical Engineering, Taishan Medical College, Taian, Shandong 271016, China

ARTICLE INFO

Article history:
Received 16 July 2013
Received in revised form 20 November 2013
Accepted 23 November 2013
Available online 3 December 2013

Keywords:
Fungal enzyme
Dismutation
Antioxidant
Thermostability
Metal binding
Oxidative stress

ABSTRACT

A manganese superoxide dismutase from the thermophilic fungus *Chaetomium thermophilum* (*Ct*MnSOD) was expressed in *Pichia pastoris* and purified to homogeneity. Its optimal temperature was 60 °C with approximately 75% of its activity retained after incubation at 70 °C for 60 min. Recombinant yeast cells carrying *C. thermophilum mnsod* gene exhibited higher stress resistance to salt and oxidative stress-inducing agents than control yeast cells. In an effort to provide structural insights, *Ct*MnSOD was crystallized and its structure was determined at 2.0 Å resolution. The overall architecture of *Ct*MnSOD was found similar to other MnSODs with highest structural similarities obtained against a MnSOD from the thermotolerant fungus *Aspergillus fumigatus*. In order to explain its thermostability, structural and sequence analysis of *Ct*MnSOD with other MnSODs was carried out. An increased number of charged residues and an increase in the number of intersubunit salt bridges and the Thr:Ser ratio were identified as potential reasons for the thermostability of *Ct*MnSOD.

1. Introduction

Manganese superoxide dismutase (MnSOD) belongs to the superoxide dismutase (SODs, EC 1.15.1.1) family of metalloenzymes that protect the cells against the harmful effects of $O_2^{\bullet-}$ by catalyzing the disproportionation of $O_2^{\bullet-}$ to less toxic H_2O_2 and O_2. In addition to MnSOD, three other main classes of SODs have been identified based on their active site metal requirements and protein fold: copper zinc SOD (Cu,ZnSOD), iron SOD (FeSOD), and nickel SOD (NiSOD). The enzymatic reaction in each of these enzymes proceeds through the cyclic reduction and reoxidation of the bound metal ion. FeSODs and MnSODs are highly homologous but they exhibit strict metal specificity despite their high similarity on the three-dimensional structure. Only a small number of Mn/FeSODs, known as cambialistic SODs, are completely active in the presence of either Mn(III) or Fe(III) [1].

MnSOD is found in mitochondria as an essential metalloenzyme for the survival of all aerobic organisms from bacteria to humans [2]. The enzyme is also present in many anaerobes for their protection during exposure to aerobic conditions. Mice deficient in mitochondrial MnSOD exhibit several pathological features, including myocardial injury and neurogeneration, which lead to their death within 5–21 days after birth [3]. In addition, MnSOD has been found to act as a tumor-suppressor by modulating ROS levels in cancer cells [4].

Crystal structures of MnSODs have been determined from various organisms, including *Aeropyrum pernix* K1 [5], yeast (*Saccharomyces cerevisiae* and *Candida albicans*) MnSOD [6], *Escherichia coli* [7] in Mn-bound and in the apo-form [8], *Deinococcus radiodurans* [9], *Caenorhabditis elegans* [10], human [11], *Bacillus stearothermophilus* [12], *Thermus thermophilus* [13], *Propionibacterium shermanii* [14], *Bacillus halodenitrificans* [15], and *Aspergillus fumigatus* [16]. The enzyme exhibits a general fold that consists of a α-hairpin N-terminal domain and a C-terminal α/β domain. The enzyme is found as either a dimer or a tetramer. Structural analysis has shown that the main difference between dimeric and tetrameric MnSODs is in the α-hairpin N-terminal domain of the enzyme. In tetrameric MnSODs, an extended conformation and the lack of an additional helix allow favorable interactions between subunits to form a dimer of dimers [10].

The role of ROS in various diseases has led to the suggestion that SODs could be employed as therapeutic agents [17]. The presence of MnSOD in mitochondria as a major scavenging enzyme for ROS has prompted research into MnSOD mimics that could enter mitochondria and mimic MnSOD [2,4]. In addition, SODs have been suggested for use in various industrial applications, such as in food industry as antioxidant [18]. For their effective use, however, the enzymes have to exhibit functional and structural stability under harsh conditions. Recently, *T.*

Abbreviations: *Ct*MnSOD, *Chaetomium thermophilum* manganese superoxide dismutase; SAA, solvent accessible area; RSAA, relative solvent accessible area.

* Turku Centre for Biotechnology, University of Turku, BioCity, Turku 20521, Finland. Tel.:+358 2 3338012.
E-mail address: tassos.papageorgiou@btk.fi (A.C. Papageorgiou).
[1] Present address: Department of Biochemistry, University of Oulu, Oulu 90014, Finland.

1570-9639/$ – see front matter © 2013 Elsevier B.V. All rights reserved.
http://dx.doi.org/10.1016/j.bbapap.2013.11.014

thermophilus MnSOD was purified and covalently immobilized onto supermagnetic nanoparticles for creation of nanosensors [19]. The immobilized MnSOD exhibited better resistance to temperature, pH, metal ions, enzyme inhibitors, and detergents.

The recent genome sequence of the thermophilic fungus *Chaetomium thermophilum* has drawn attention to the protein properties of this thermophile and its use as a model system for biophysical studies [20]. Moreover, as the only eukaryotic organisms which can grow above 45 °C, thermophilic fungi have received considerable scientific and commercial interest in recent years as a source of new thermostable enzymes [21,22]. Thus, studies on enzymes produced by thermophilic fungi could be beneficial to several applications in which elevated temperatures are required. Here, we report the crystal structure of a thermostable MnSOD from *C. thermophilum* (*Ct*MnSOD). The presented detailed analysis shows some common features of *Ct*MnSOD with other thermophilic and hyperthermophilic MnSODs and structural similarities with a MnSOD from another thermophilic fungus.

2. Materials and methods

2.1. Cloning, expression and purification

2.1.1. Construction of the expression plasmid

*Ct*MnSOD gene (European Nucleotide Archive id: JN018420) was isolated firstly from *C. thermophilum* CT2 by RT-PCR and Tail-PCR. Based on the *Ct*MnSOD gene sequence, a pair of specific primers containing restriction sites (5′-CCGAATTCAAGGCCACCCTGCCCGAC-3′ (*Eco*RI); 5′-GGGCGGCCGCTTAGGCCTTCTCAAAGCGCT-3′ (*Not*I)) was designed to amplify the complementary DNA (cDNA) sequence encoding the mature MnSOD (197 amino acids). The PCR product was digested with restriction enzymes, and subcloned into the expression vector pPIC9K (Invitrogen). The positive recombinants were confirmed by PCR amplification with a pair of primers corresponding to 5′AOX1 sequencing primer and 3′AOX1 sequencing primer (Invitrogen). The resulting recombinant plasmids were designated as pPIC9K/*mnsod*. The expression plasmid pPIC9K/*mnsod* was subsequently confirmed by PCR analysis, restriction analysis, and DNA sequencing.

2.1.2. Transformation of Pichia pastoris GS115 and screening of transformants

The *Sac*I-linearized recombinant plasmid pPIC9K/*mnsod* was transformed into *P. pastoris* GS115 by electroporation with Eppendorf Electroporartor 2510. For the verification of gene integration into the *Pichia* genome, genomic DNA of a number of transformants was isolated. PCR amplifications were carried out based on genomic DNA and using primers corresponding to α-Factor Sequencing Primer and 3′AOX1 Sequencing primer (Invitrogen).

2.1.3. Induced expression

The transformants were grown in BMGY at 28 °C until A_{600} reached 1–2. The cells were harvested by centrifugation at 5000 *g* for 5 min, and then cultured in BMMY. The expression was induced by adding 1% methanol into BMMY, using another cell culture with no added methanol as a control. Aliquots of each culture were removed at 24 h intervals and induced expression of the recombinant *Ct*MnSOD was detected by SDS-PAGE.

2.1.4. Purification of CtMnSOD

Transformed yeast was cultured at 28 °C for 7 days in BMMY medium according to the *Pichia* Expression System Kit (Invitrogen). The culture filtrate was centrifuged at 10000 *g* for 10 min at 4 °C, and the resultant supernatant was dialysed overnight against three changes of 50 mM Tris–HCl (pH 8.0, buffer A). The dialysed sample was loaded onto a DEAE-Sepharose column (1 × 20 cm) equilibrated with buffer A. After the column was washed with five column volumes of buffer A, a 240 ml linear gradient of NaCl (0–0.3 M in buffer A) was applied at a flow rate of 60 ml/h. The volume of each fraction was 3 ml. Fractions with *Ct*MnSOD activity were collected. The purity of the recombinant *Ct*MnSOD was determined by SDS-PAGE.

2.2. Thermal stability

The optimum reaction temperature was measured in 50 mM NaH_2PO4–Na_2HPO4 (pH 7.5) buffer at 30–90 °C. The retaining activity was examined at 60–90 °C in the same buffer without substrate. Samples were removed at fixed (1 h) intervals and allowed to cool in an ice bath. Residual *Ct*MnSOD activities for evaluating the thermal stability were tested under standard assay conditions [23].

2.3. Antioxidant activity

Control strains carrying empty pPIC9K vector (Invitrogen) and transformant strains carrying pPIC9K/*mnsod* vector were grown on YPD medium at 28 °C for 20 h, adjusted to the same absorbance (OD_{600}) and then serially ten-fold diluted to 10^{-1}, 10^{-2}, 10^{-3}, 10^{-4} and 10^{-5} in sterile water. Samples, 3 μl of each dilution, were spotted on plates supplemented with various concentrations of paraquat, H_2O_2, and NaCl, and incubated for 3 days at 28 °C. The control consisted of a plate without any stressful agents.

2.4. Crystallization

Prior to crystallization, the enzyme was concentrated to ~10 mg ml^{-1} in 10 mM Tris–HCl buffer, pH 8.0. Initial crystallization conditions were established with the PACT screen (Qiagen) in 96-well plate using the sitting-drop vapor diffusion method. Crystals appeared in condition 54 (0.2 M sodium formate, 20% w/v PEG3350) and were further optimized by the hanging-drop vapor-diffusion method in Linbro 24-well cell-culture plates. The drops consisted of 2 μl of protein solution (10 mg/ml in 10 mM Tris–HCl, pH 8.0) mixed with 2 μl of reservoir solution (0.2 M sodium formate, 16% w/v PEG3350). The drops were equilibrated against 800 μl of reservoir solution at 16 °C. Crystals appeared after ~2 weeks.

2.5. Data collection

For data collection, a single crystal was briefly soaked in a reservoir solution supplemented with 20% v/v glycerol as a cryoprotectant. The crystal was subsequently placed in a stream of gaseous N_2 at 100 K. A total of 300 images were recorded on a 165 mm MARCCD (station X13 at EMBL-Hamburg, c/o DESY). The X-ray wavelength, the crystal-to-detector distance and the rotation range were set to 0.81230 Å, 185 mm and 0.35°, respectively. All data were processed, scaled and integrated with XDS [24]. The crystal belonged to space group $P6_1$/$P6_5$ with unit cell dimensions of 69.1 × 69.1 × 300.5 Å (γ = 120°). Assuming 4 molecules in the asymmetric unit, the solvent content was 38.9%.

2.6. Structure determination and refinement

Initial phases were obtained by molecular replacement using human mitochondrial MnSOD variant (PDB id: 1var) [25] as a search model in PHASER [26]. The search model was modified according to sequence alignment by pruning non-conserved residues to the Cβ-atom with CHAINSAW [27]. Both $P6_1$ and $P6_5$ space groups were tested and the best solution was found in space group $P6_1$ (RFZ = 4.3, TFZ = 26.7, LLG = 876, total LLG = 999). Model building was carried out with PhenixAutobuild in PHENIX [28] resulting in an R_{work} of 22.8% (R_{free} = 25.6%), and 756 residues in 8 fragments. The structure was displayed and manually rebuilt using COOT [29]. Further refinement was carried out with PHENIX. Twinning operators were applied as the data were subsequently found merohedrally twinned according to the twin law "h,−h − k,−l". The estimated twin fraction calculated by Xtriage was 0.268 (Britton analyses), 0.285 (H-test), and 0.222

(Maximum likelihood method). The refined twin fraction was 0.28. A new R_{free} set was subsequently generated within PHENIX using the lattice symmetry of the space group. Validation of the final structure was carried out with MOLPROBITY [30], POLYGON [31] and diagnostic tools as implemented in COOT and PHENIX. Detailed statistics of data collection and refinement are presented in Table 1.

2.7. Structural analysis

Number of residues, polar and apolar residues, and charged residues were calculated based on the protein sequence. The solvent accessible area (SAA) and solvation energy were calculated by PDBePISA [32]. The relative solvent accessible area (RSAA) was calculated as A_o/A_c where $A_c = 15 \times N^{0.866}$ and A_o the observed solvent accessible area (N is the number of atoms). In these calculations, the average N and A_o in each structure were used as given by PDBePISA owing to the presence of more than one subunit in most structures. Protein volume was calculated using CHIMERA [33].

3. Results and discussion

3.1. Purification and biochemical characterization

The molecular weight of the purified recombinant *Ct*MnSOD was about 23 kDa (Fig. 1), as expected based on the calculated molecular weight from the amino acid sequence. The enzyme was found to exhibit maximal optimum temperature at 60 °C (Fig. 2). It was thermostable at 50 and 60 °C and retained 75% of its activity after 60 min at 70 °C. The half-life of *Ct*MnSOD at 80 °C was approximately 25 min and the enzyme retained 20% activity even after 30 min at 90 °C. The recombinant *Ct*MnSOD shows therefore similar properties to the non-recombinant *Ct*MnSOD [34].

Table 1
Data collection and refinement statistics.[a]

Data collection	
Space group	*P*61
Cell dimensions (Å)	69.1 × 69.1 × 300.4 (γ = 120°)
No. of molecules/au	4
Resolution range (Å)	20.0–2.0 (2.05–2.00)
Number of measured reflections	333881 (15142)
Unique reflections	54201 (3583)
Completeness (%)	99.0 (88.8)
Mosaicity (°)	0.375
<I/σ(I)>	25.4 (4.1)
R_{merge} (%)	5.5 (35.9)
R_{meas} (%)	6.0 (40.6)
Wilson B-factor (Å^2)	29.1
Refinement	
Reflections (working/test)	54085/1988
R_{cryst}/R_{free} (%)	12.1/17.9
Protein atoms	6087
Waters	1279
Mn^{2+}	4
Na^{+}	6
RMS deviation from ideal geometry	
Bond lengths (Å)	0.007
Bond angles (°)	1.00
Ramachandran plot	
Favored residues (%)	97.0
Outliers (%)	0.0
Average B factors (Å^2)	
Protein	23.0
Waters	31.4
Mn^{2+}	17.7
Na^{+}	28.3

[a] Numbers in parentheses correspond to the highest resolution shell.

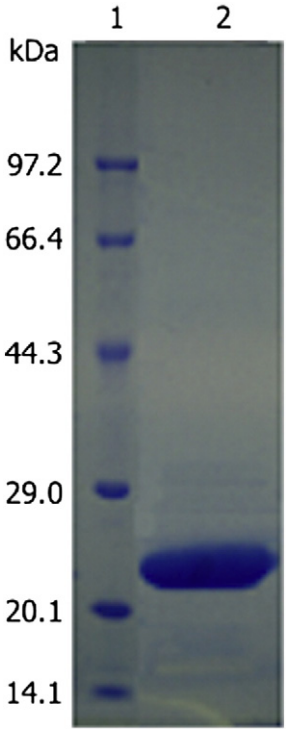

Fig. 1. SDS-PAGE of the purified recombinant *Ct*MnSOD. Lane 1, molecular weight marker; Lane 2, purified recombinant *Ct*MnSOD.

3.2. Stress protection

The recombinant yeast GS115 harboring pPIC9K/*mnsod* and control GS115 harboring empty pPIC9K were treated with different

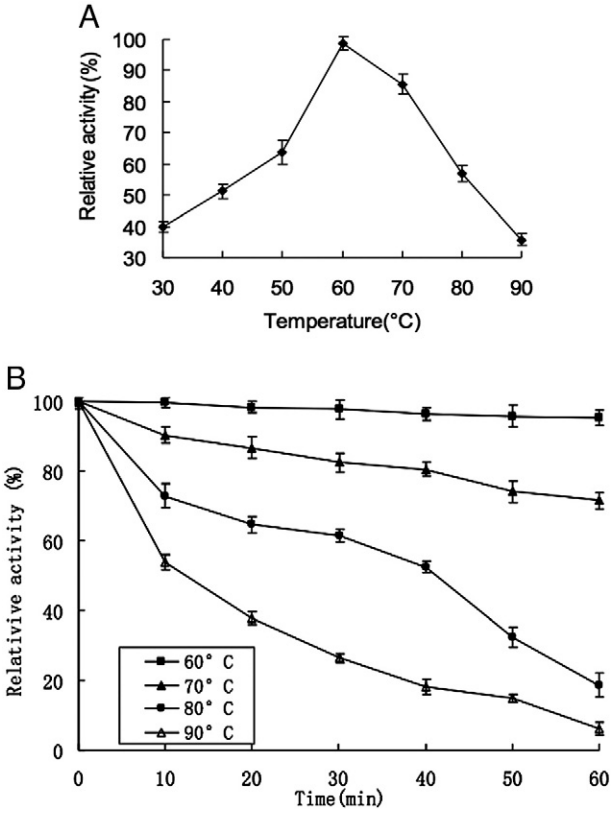

Fig. 2. (A) Optimum reaction temperature. (B) Residual activity after incubation at various temperatures. Both experiments were conducted in triplicate.

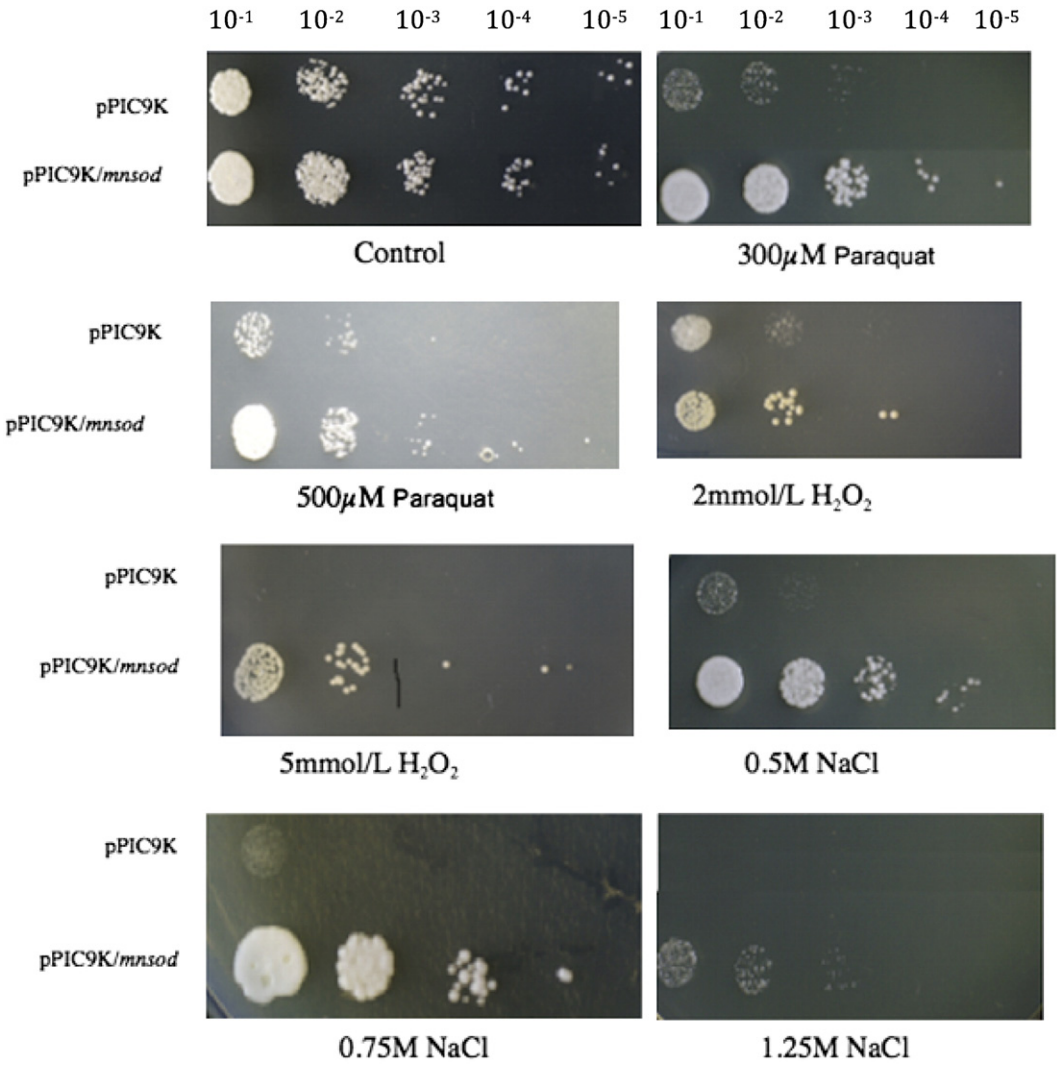

Fig. 3. Salt and oxidation resistance of recombinant yeast cells.

concentration of salt (NaCl) [35] and oxidative stress-inducing agents, such as paraquat and H_2O_2. The results revealed that the recombinant yeast cells have a higher stress resistance than the control cells (Fig. 3). The results also suggest that the *C. thermophilum mnsod* gene has the ability of conferring salt and oxidative stress resistance and may be useful in the development of transgenic plants with enhanced tolerance to salt and oxidative stress. The mechanism, however, of the protection needs to be further investigated.

3.3. Structure determination and quality of the structure

The structure of *Ct*MnSOD was determined by molecular replacement to a resolution of 2.0 Å. The final R_{work} and R_{free} were 12.1% and 17.9%, respectively. Four molecules (A–D) of *Ct*MnSOD were found in the crystallographic asymmetric unit with overall B-factors between 21.6 and 24.1 $Å^2$. Two residues (C:Arg173, D:Arg111) were modeled with alternative conformations. The coordinate error based on the diffraction precision index [36] is 0.13 Å. The OH group of Tyr9 residues in each subunit was not modeled owing to the lack of electron density, most likely as a result of radiation damage [37].

3.4. Overall structure

Similarly to other MnSODs, *Ct*MnSOD forms a homotetramer of 222-symmetry in the asymmetric unit (Fig. 4A). The oligomerization stage in the crystals is therefore in agreement with gel filtration experiments [34]. Structural superposition of the four subunits shows a root mean square deviation (rmsd) in Cα-atoms of 0.26–0.33 Å, suggesting no significant deviations in subunit structure. The overall architecture is similar to that of other MnSODs and consists of two domains: an N-terminal α-helical domain and a C-terminal α/β domain (Fig. 4B). The N-terminal domain has two long helices (α1: 20–51; α3: 54–80). The first 1–19 residues display an extended structure that is packed against helices α1 and α3. A bulge in helix α3 is caused by the presence of a Pro residue at position 62. An extra helix, α2, found between α1 and α3 in some MnSODs is absent in *Ct*MnSOD. This region is highly variable with extensive deletions or insertions and has been suggested to play a role in allowing the subunits to form a dimer of dimers [10]. Accordingly, several amino acids have been proposed to affect the dimer–tetramer formation [38].

The C-terminal domain contains six α-helices (Gly94-Phe104; Phe107-Thr119; Glu163-Ala165; Tyr167-Tyr170; Lys174-Asn183; Trp187-Glu195) and three β-strands (Gly125-Asp132; Leu138-Ala144; Leu153-Asp160). A PDB search using PDBeFold [39] revealed similarities of *Ct*MnSOD with *A. fumigatus* MnSOD [16]. The rmsd between the two structures was 0.78 Å, corresponding to 56% sequence identity for 196 aligned residues. Furthermore, a structure-based sequence alignment with mesophilic and thermophilic MnSODs was carried out (Fig. 5), resulting in rmsd values ranging from 0.3 to 1.4 Å (overall rmsd = 1.0 Å). The superimposed MnSODs are shown in Fig. 6,

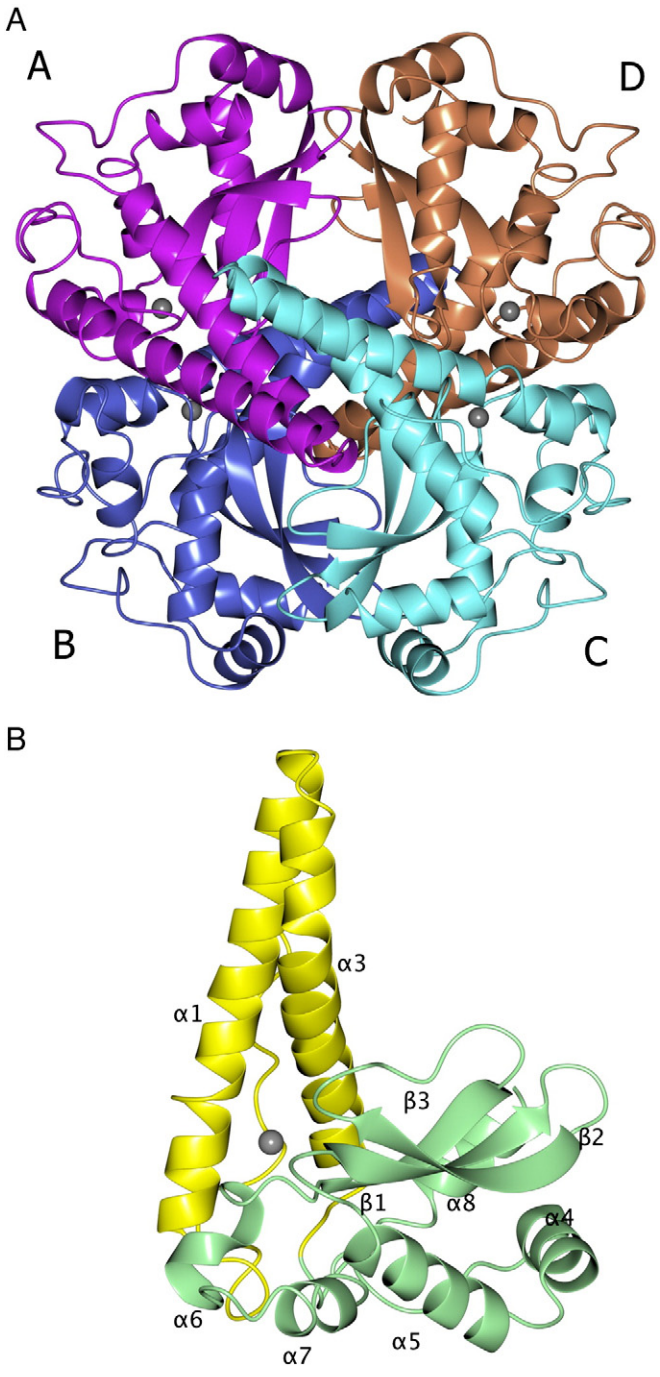

Fig. 4. (A) Ribbon diagram of the *Ct*MnSOD tetramer. Each subunit is colored in a different color and labeled. Mn^{2+} ions are shown as gray spheres. (B) Ribbon diagram of *Ct*MnSOD subunit. The two domains are colored in yellow and light green. The figure was drawn with CCP4mg [54].

confirming the regions of high variability mainly in the loop regions of the structures and the N- and C-termini.

3.5. Active site

Examination of the electron density map showed strong density (up to 20σ in $F_o - F_c$ electron density maps) corresponding to bound Mn^{2+} ions. The protein ligands for the Mn ions are His26 and His74 from the N-terminal domain, and Asp160 and His164 from the C-terminal domain (Fig. 7). In addition, each Mn^{2+} ion is coordinated by a water or hydroxyl ion, resulting in five-coordinated trigonal bipyramidal geometry. As observed also in other MnSODs, the Mn^{2+}-binding site is located near the end of a solvent-filled tunnel and terminates at His30 and Tyr34, which are conserved amongst MnSODs. A cluster of conserved and mostly hydrophobic residues surrounds the Mn-binding site (Phe77, Trp78, Trp126, Tyr166, Tyr167, Tyr177) while the substrate-binding site next to the Mn-binding site is formed by His31, Tyr34, His74, and Trp78.

3.6. Subunit interface

The *Ct*MnSOD tetramer has two, practically similar, major interfaces: A–B and C–D. Each of these interfaces covers 890 $Å^2$ of SAA of each subunit, corresponding to 9.2% of the total SAA of the subunit and involves 19 residues from subunit A and 22 residues from subunit B. The regions that are involved in the interface formation are 21–33, 62–66, 122–124, and 162–173. There are 11 salt bridges (Supplementary Table 1) and 15 hydrogen bonds (Supplementary Table 2). Salt bridges are formed between Arg21-Glu171 and Glu163-His164. The latter pair is highly conserved between MnSODs. In contrast, Arg21 and Glu171 show variability amongst different MnSODs. For example, in *T. thermophilus* MnSOD, Arg21 is replaced by Lys or by either Glu or Gln in other MnSODs. However, in *Pyrobaculum aerophilum* MnSOD (PDB id: 3evk), *A. pernix* cambialistic SOD (PDB id: 3ak2), and *C. elegans* MnSOD (PDB id: 3dc6) the residues are swapped while in *Sulfolobus solfataricus* FeSOD (PDB id: 1wb8) there is an Asp residue instead of Glu but nevertheless the Lys is present to preserve the interaction. A prominent hydrogen bond formed between Tyr167 from one subunit and His30 from the second subunit is highly conserved amongst MnSODs and plays a role in structure and reactivity. Mutation of either residue has been found to reduce activity by 30–40% [40].

The A–B subunit interface on *Ct*MnSOD shows the highest similarities with that of *A. fumigatus* MnSOD with sequence identity of 56% and a Q-score of 0.899. The interface of a mitochondrial *S. cerevisiae* MnSOD (PDB id: 3lsu) [6] was found in the second place of interface similarity. Additional interfaces in tetramer formation include C–A and B–D. Each of these interfaces buries ~811 $Å^2$ of SAA from each subunit (8.2% of the total subunit SAA) and involves residues mainly from 50 to 72, leading to a four-helix bundle. As with the A–B and C–D interfaces, C–A and B–D show also similarities with the *A. fumigatus* MnSOD corresponding interfaces (seq. identity ~55.7%).

3.7. Comparison with other MnSODs and thermostability

Comparison of thermal stability of *Ct*MnSOD with other MnSODs is shown in Table 2. Several factors implicated in protein thermostability were examined (Supplementary Table 3). Calculation of the percentage of charged residues (Arg + Lys + Glu + Asp) revealed a slight increase as shown also in other thermophilic MnSODs. In addition, the Thr:Ser ratio was found elevated in accordance to similar trend found in other MnSODs from thermophilic organisms. The number of salt bridges at the interface of *Ct*MnSOD is comparable to that found in other thermophilic MnSODs and considerably higher than that in mesophilic enzymes. In regard to RSAA, no clear trend was identified in the examined enzymes although small RSAA numbers have been suggested to contribute to the thermostability of MnSODs [41,42]. The volume/residue ratio has been found increased in thermophilic MnSODs [42] but in *Ct*MnSOD it appears to exhibit more similarities to that of the mesophilic MnSODs. Thus, a combination of various factors and structural variations may contribute to the thermostability of *Ct*MnSOD and other MnSODs, in agreement with previous observations in other enzyme families [43–45].

4. Conclusions

*Ct*MnSOD was successfully expressed and purified in *P. pastoris*. The recombinant enzyme showed similar thermostability as the non-

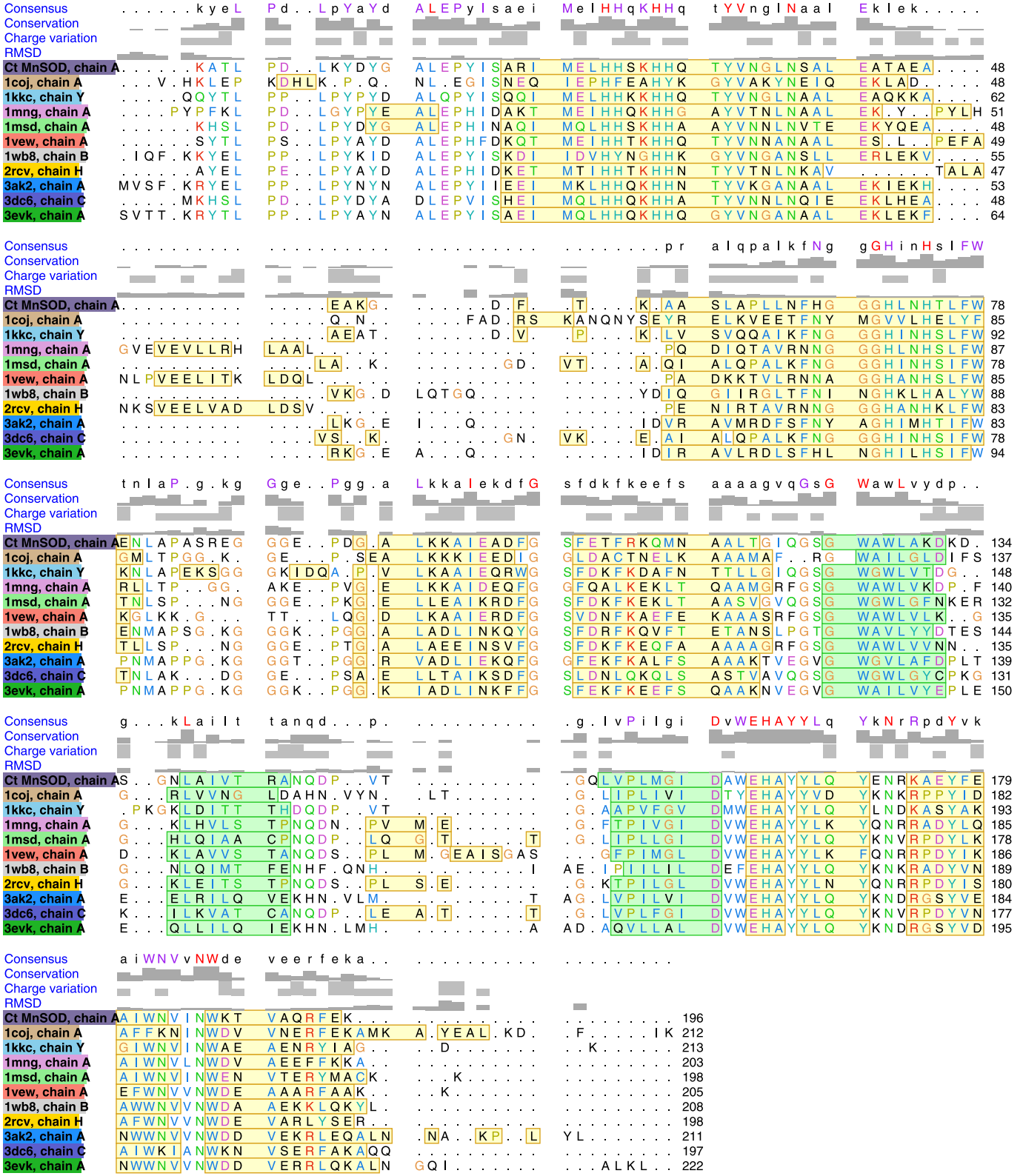

Fig. 5. Structure-based alignment of MnSODs from various species. The program CHIMERA was used. Light green and orange depict regions of β-strands and α-helices, respectively. Residue numbering for each structure is shown on the right of the sequence. The subunit used from each structure for the structure-based sequence alignment is indicated and was chosen by CHIMERA for optimal results. Residue coloring is based on Clustal X one-letter residue coloring as implemented in CHIMERA. The MnSODs used are from the following species: 3evk, *Pyrobaculum aerophilum* [55]; 3ak2, *Aeropyrum pernix* [5]; 1wb8, *Sulfolobus solfataricus* [42]; 1coj, *Aquifex pyrophilus* [48]; 1mng, *Thermus thermophilus* HB27 [56]; 4br6, *Chaetomium thermophilum*; 2rcv, *Bacillus subtilis* [57]; 1kkc, *Aspergillus fumigatus* [16]; 1msd, human mitochondrial [58]; 3dc6, *Caenorhabditis elegans* [10]; 1vew, *Escherichia coli* [7].

recombinant *Ct*MnSOD and conferred salt and oxidation resistance to recombinant yeast cells. The crystal structure of *Ct*MnSOD showed the typical architecture of MnSODs. The enzyme crystallized as a tetramer in the asymmetric unit in accordance to its oligomerization stage in solution. An elevated number of charged residues, an increase in the number of intersubunit salt bridges, and an increase in the Thr:Ser

Fig. 6. Structural superposition of various MnSODs onto *Ct*MnSOD. The coloring scheme is the same as in Fig. 5.

ratio are suggested to contribute to the thermostability of *Ct*MnSOD. Structural similarities with a MnSOD from the thermophilic fungus *A. fumigatus* may indicate some common features in fungal MnSODs.

Table 2
Thermal stability of MnSODs.

Origin	T_{opt}[a] (°C)	Stability[b] (°C)	References	Oligomerization
Pyrobaculum aerophilum	100	95–100	[46]	Tetramer
Aeropyrum pernix	90–95	105	[47]	Tetramer[c]
Sulfolobus solfataricus	87	–	[42]	Tetramer
Aquifex pyrophilus	85	95–100	[48]	Tetramer
Thermus thermophilus HB27	65	80 and 90	[49]	Dimer
Chaetomium thermophilum	60	50 and 60	[34]	Tetramer
Bacillus subtilis	37	60	[50]	Dimer
Aspergillus fumigatus	37	70	[51]	Tetramer
Human mitochondrial	37	–	[52]	Tetramer
Escherichia coli	37	–	[42]	Dimer
Caenorhabditis elegans	15–25	–	[53]	Dimer

[a] Optimum growth temperature of the source organism (T_{opt}).
[b] As determined by the residual activity in enzymatic assays.
[c] Initial reports suggested a dimer, but ultracentrifugation experiments confirmed the presence of a tetramer in solution, similarly to the crystal.

Acknowledgements

This work was partially supported by the Chinese National Nature Science Foundation, the Chinese National Program for High Technology, Research and Development, the Chinese Project of Transgenic Organisms, the Chinese National Special Fund of Sea Renewable Energy Sources and the Shandong Natural Science Fund. A.C.P thanks the Academy of Finland (grant no. 121278) and Turku University Foundation for financial support, and Biocenter Finland for infrastructure support. Access to EMBL-Hamburg c/o DESY was provided by the European Community's Seventh Framework Programme (FP7/2007-2013) under grant agreements 226716 and 283570 (BioStruct-X project).

Appendix A. Supplementary data

Supplementary data to this article can be found online at http://dx.doi.org/10.1016/j.bbapap.2013.11.014.

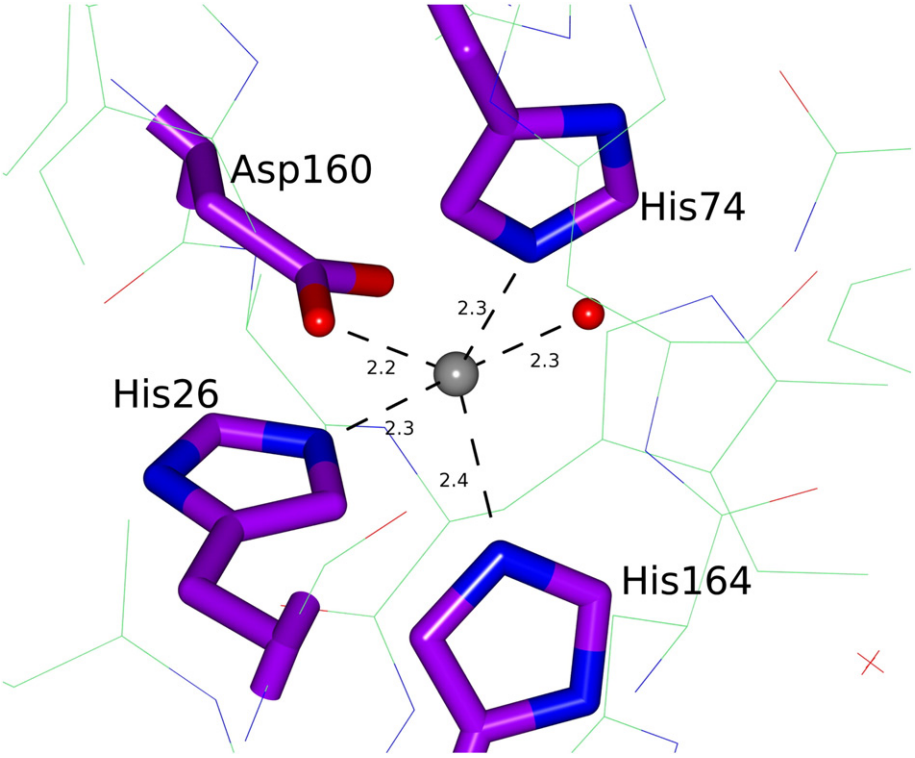

Fig. 7. Close-up view of the Mn-binding site in subunit A.

References

[1] W.F. Beyer, I. Fridovich, In vivo competition between iron and manganese for occupancy of the active site region of the manganese-superoxide dismutase of *Escherichia coli*, J. Biol. Chem. 266 (1991) 303–308.

[2] S. Miriyala, I. Spasojevic, A. Tovmasyan, D. Salvemini, Z. Vujaskovic, D. St Clair, I. Batinic-Haberle, Manganese superoxide dismutase, MnSOD and its mimics, Biochim. Biophys. Acta 1822 (2012) 794–814.

[3] R.M. Lebovitz, H. Zhang, H. Vogel, J. Cartwright, L. Dionne, N. Lu, S. Huang, M.M. Matzuk, Neurodegeneration, myocardial injury, and perinatal death in mitochondrial superoxide dismutase-deficient mice, Proc. Natl. Acad. Sci. U. S. A. 93 (1996) 9782–9787.

[4] A.K. Holley, S.K. Dhar, Y. Xu, D.K. St Clair, Manganese superoxide dismutase: beyond life and death, Amino Acids 42 (2012) 139–158.

[5] T. Nakamura, K. Torikai, K. Uegaki, J. Morita, K. Machida, A. Suzuki, Y. Kawata, Crystal structure of the cambialistic superoxide dismutase from *Aeropyrum pernix* K1 —insights into the enzyme mechanism and stability, FEBS J. 278 (2011) 598–609.

[6] Y. Sheng, T.A. Stich, K. Barnese, E.B. Gralla, D. Cascio, R.D. Britt, D.E. Cabelli, J.S. Valentine, Comparison of two yeast MnSODs: mitochondrial *Saccharomyces cerevisiae* versus cytosolic *Candida albicans*, J. Am. Chem. Soc. 133 (2011) 20878–20889.

[7] R.A. Edwards, H.M. Baker, M.M. Whittaker, J.W. Whittaker, G.B. Jameson, E.N. Baker, Crystal structure of *Escherichia coli* manganese superoxide dismutase at 2.1-Å resolution, J. Biol. Inorg. Chem. 3 (1998) 161–171.

[8] M.M. Whittaker, T.F. Lerch, O. Kirillova, M.S. Chapman, J.W. Whittaker, Subunit dissociation and metal binding by *Escherichia coli* apo-manganese superoxide dismutase, Arch. Biochem. Biophys. 505 (2011) 213–225.

[9] R.J. Dennis, E. Micossi, J. McCarthy, E. Moe, E.J. Gordon, S. Kozielski-Stuhrmann, G.A. Leonard, S. McSweeney, Structure of the manganese superoxide dismutase from *Deinococcus radiodurans* in two crystal forms, Acta Crystallogr. Sect. F: Struct. Biol. Cryst. Commun. 62 (2006) 325–329.

[10] C.H. Trinh, T. Hunter, E.E. Stewart, S.E.V. Phillips, G.J. Hunter, Purification, crystallization and X-ray structures of the two manganese superoxide dismutases from *Caenorhabditis elegans*, Acta Crystallogr. Sect. F: Struct. Biol. Cryst. Commun. 64 (2008) 1110–1114.

[11] J. Zheng, J.F. Domsic, D. Cabelli, R. McKenna, D.N. Silverman, Structural and kinetic study of differences between human and *Escherichia coli* manganese superoxide dismutases, Biochemistry 46 (2007) 14830–14837.

[12] M.W. Parker, C.C.F. Blake, Crystal structure of manganese superoxide dismutase from *Bacillus stearothermophilus* at 2.4 Å resolution, J. Mol. Biol. 199 (1988) 649–661.

[13] M.L. Ludwig, A.L. Metzger, K.A. Pattridge, W.C. Stallings, Manganese superoxide dismutase from *Thermus thermophilus*. A structural model refined at 1.8 Å resolution, J. Mol. Biol. 219 (1991) 335–358.

[14] B. Meier, F. Parak, A. Desideri, G. Rotilio, Comparative stability studies on the iron and manganese forms of the cambialistic superoxide dismutase from *Propionibacterium shermanii*, FEBS Lett. 414 (1997) 122–124.

[15] J. Liao, M.Y. Liu, T. Chang, M. Li, J. Le Gall, L.L. Gui, J.P. Zhang, T. Jiang, D.C. Liang, W.R. Chang, Three-dimensional structure of manganese superoxide dismutase from *Bacillus halodenitrificans*, a component of the so-called "green protein", J. Struct. Biol. 139 (2002) 171–180.

[16] S. Flückiger, P.R.E. Mittl, L. Scapozza, H. Fijten, G. Folkers, M.G. Grütter, K. Blaser, R. Crameri, Comparison of the crystal structures of the human manganese superoxide dismutase and the homologous *Aspergillus fumigatus* allergen at 2-A resolution, J. Immunol. 168 (2002) 1267–1272.

[17] J.J.P. Perry, L. Fan, J.A. Tainer, Developing master keys to brain pathology, cancer and aging from the structural biology of proteins controlling reactive oxygen species and DNA repair, Neuroscience 145 (2007) 1280–1299.

[18] A. Boonmee, C. Srisomsap, A. Karnchanatat, An antioxidant protein in *Curcuma comosa* Roxb. Rhizomes, Food Chem. 124 (2011) 476–480.

[19] C. Song, L. Sheng, X. Zhang, Preparation and characterization of a thermostable enzyme (Mn-SOD) immobilized on supermagnetic nanoparticles, Appl. Microbiol. Biotechnol. 96 (2012) 123–132.

[20] S. Amlacher, P. Sarges, D. Flemming, V. van Noort, R. Kunze, D.P. Devos, M. Arumugam, P. Bork, E. Hurt, Insight into structure and assembly of the nuclear pore complex by utilizing the genome of a eukaryotic thermophile, Cell 146 (2011) 277–289.

[21] R. Maheshwari, G. Bharadwaj, M.K. Bhat, Thermophilic fungi: their physiology and enzymes, Microbiol. Mol. Biol. Rev. 64 (2000) 461–488.

[22] D.-C. Li, A.-N. Li, A.C. Papageorgiou, Cellulases from thermophilic fungi: recent insights and biotechnological potential, Enzym. Res. (2011) 308730(Article ID).

[23] R. Stewart, J. Bewley, Lipid peroxidation associated with accelerated aging of soybean axes, Plant Physiol. 65 (1980) 245–248.

[24] W. Kabsch, XDS, Acta Crystallogr. D Biol. Crystallogr. 66 (2010) 125–132.

[25] G.E. Borgstahl, H.E. Parge, M.J. Hickey, M.J. Johnson, M. Boissinot, R.A. Hallewell, J.R. Lepock, D.E. Cabelli, J.A. Tainer, Human mitochondrial manganese superoxide dismutase polymorphic variant Ile58Thr reduces activity by destabilizing the tetrameric interface, Biochemistry 35 (1996) 4287–4297.

[26] A. McCoy, R. Grosse-Kunstleve, P. Adams, M. Winn, L. Storoni, R. Read, Phaser crystallographic software, J. Appl. Crystallogr. 40 (2007) 658–674.

[27] N. Stein, CHAINSAW: a program for mutating pdb files used as templates in molecular replacement, J. Appl. Crystallogr. 41 (2008) 641–643.

[28] P.D. Adams, P.V. Afonine, G. Bunkóczi, V.B. Chen, I.W. Davis, N. Echols, J.J. Headd, L.-W. Hung, G.J. Kapral, R.W. Grosse-Kunstleve, A.J. McCoy, N.W. Moriarty, R. Oeffner, R.J. Read, D.C. Richardson, J.S. Richardson, T.C. Terwilliger, P.H. Zwart, PHENIX: a comprehensive Python-based system for macromolecular structure solution, Acta Crystallogr. D Biol. Crystallogr. 66 (2010) 213–221.

[29] P. Emsley, K. Cowtan, Coot: model-building tools for molecular graphics, Acta Crystallogr. D Biol. Crystallogr. 60 (2004) 2126–2132.

[30] S. Lovell, I. Davis, W. Arendall, P. de Bakker, J. Word, M. Prisant, J. Richardson, D. Richardson, Structure validation by Calpha geometry: phi, psi and Cbeta deviation, Proteins 50 (2003) 437–450.

[31] L. Urzhumtseva, P.V. Afonine, P.D. Adams, A. Urzhumtsev, Crystallographic model quality at a glance, Acta Crystallogr. D Biol. Crystallogr. 65 (2009) 297–300.

[32] E. Krissinel, K. Henrick, Inference of macromolecular assemblies from crystalline state, J. Mol. Biol. 372 (2007) 774–797.

[33] E.C. Meng, E.F. Pettersen, G.S. Couch, C.C. Huang, T.E. Ferrin, Tools for integrated sequence–structure analysis with UCSF Chimera, BMC Bioinforma. 7 (2006) 339.

[34] F.-X. Guo, E. Shi-Jin, S.-A. Liu, J. Chen, D.-C. Li, Purification and characterization of a thermostable MnSOD from the thermophilic fungus *Chaetomium thermophilum*, Mycologia 100 (2008) 375–380.

[35] F. Madeo, E. Herker, S. Wissing, H. Jungwirth, T. Eisenberg, K.-U. Fröhlich, Apoptosis in yeast, Curr. Opin. Microbiol. 7 (2004) 655–660.

[36] D.W.J. Cruickshank, Remarks about protein structure precision, Acta Crystallogr. D Biol. Crystallogr. 55 (1999) 583–601.

[37] E.F. Garman, Radiation damage in macromolecular crystallography: what is it and why should we care? Acta Crystallogr. D Biol. Crystallogr. 66 (2010) 339–351.

[38] R. Wintjens, C. Noël, A.C.W. May, D. Gerbod, F. Dufernez, M. Capron, E. Viscogliosi, M. Rooman, Specificity and phenetic relationships of iron- and manganese-containing superoxide dismutases on the basis of structure and sequence comparisons, J. Biol. Chem. 279 (2004) 9248–9254.

[39] E. Krissinel, K. Henrick, Secondary-structure matching (SSM), a new tool for fast protein structure alignment in three dimensions, Acta Crystallogr. D Biol. Crystallogr. 60 (2004) 2256–2268.

[40] R.A. Edwards, M.M. Whittaker, J.W. Whittaker, E.N. Baker, G.B. Jameson, Removing a hydrogen bond in the dimer interface of *Escherichia coli* manganese superoxide dismutase alters structure and reactivity, Biochemistry 40 (2001) 4622–4632.

[41] M.K. Chan, S. Mukund, A. Kletzin, M.W. Adams, D.C. Rees, Structure of a hyperthermophilic tungstopterin enzyme, aldehyde ferredoxin oxidoreductase, Science 267 (1995) 1463–1469.

[42] T. Ursby, B.S. Adinolfi, S. Al-Karadaghi, E. De Vendittis, V. Bocchini, Iron superoxide dismutase from the archaeon *Sulfolobus solfataricus*: analysis of structure and thermostability, J. Mol. Biol. 286 (1999) 189–205.

[43] L.D. Unsworth, J. van der Oost, S. Koutsopoulos, Hyperthermophilic enzymes—stability, activity and implementation strategies for high temperature applications, FEBS J. 274 (2007) 4044–4056.

[44] S. Trivedi, H.S. Gehlot, S.R. Rao, Protein thermostability in Archaea and *Eubacteria*, Genet. Mol. Res. 5 (2006) 816–827.

[45] M. Sadeghi, H. Naderi-Manesh, M. Zarrabi, B. Ranjbar, Effective factors in thermostability of thermophilic proteins, Biophys. Chem. 119 (2006) 256–270.

[46] M.M. Whittaker, J.W. Whittaker, Recombinant superoxide dismutase from a hyperthermophilic archaeon, *Pyrobaculum aerophilium*, J. Biol. Inorg. Chem. 5 (2000) 402–408.

[47] S. Yamano, Y. Sako, N. Nomura, T. Maruyama, A cambialistic SOD in a strictly aerobic hyperthermophilic archaeon, *Aeropyrum pernix*, J. Biochem. 126 (1999) 218–225.

[48] J.H. Lim, Y.G. Yu, Y.S. Han, S. Cho, B.Y. Ahn, S.H. Kim, Y. Cho, The crystal structure of an Fe-superoxide dismutase from the hyperthermophile *Aquifex pyrophilus* at 19 A resolution: structural basis for thermostability, J. Mol. Biol. 270 (1997) 259–274.

[49] J. Liu, M. Yin, H. Zhu, J. Lu, Z. Cui, Purification and characterization of a hyperthermostable Mn-superoxide dismutase from *Thermus thermophilus* HB27, Extremophiles 15 (2011) 221–226.

[50] T. Inaoka, Y. Matsumura, T. Tsuchido, Molecular cloning and nucleotide sequence of the superoxide dismutase gene and characterization of its product from *Bacillus subtilis*, J. Bacteriol. 180 (1998) 3697–3703.

[51] M.D. Holdom, R.J. Hay, A.J. Hamilton, Purification, N-terminal amino acid sequence and partial characterization of a Cu, Zn superoxide dismutase from the pathogenic fungus *Aspergillus fumigatus*, Free Radic. Res. 22 (1995) 519–531.

[52] V.J. Lévêque, M.E. Stroupe, J.R. Lepock, D.E. Cabelli, J.A. Tainer, H.S. Nick, D.N. Silverman, Multiple replacements of glutamine 143 in human manganese superoxide dismutase: effects on structure, stability, and catalysis, Biochemistry 39 (2000) 7131–7137.

[53] T. Hunter, W.H. Bannister, G.J. Hunter, Cloning, expression, and characterization of two manganese superoxide dismutases from *Caenorhabditis elegans*, J. Biol. Chem. 272 (1997) 28652–28659.

[54] S. McNicholas, E. Potterton, K.S. Wilson, M.E.M. Noble, Presenting your structures: the *CCP4mg* molecular-graphics software, Acta Crystallogr. D Biol. Crystallogr. 67 (2011) 386–394.

[55] S. Lee, Crystal structure of the metal-bound superoxide dismutase from *Pyrobaculum aerophilum* and comparison with the metal-free form, Bull. Korean Chem. Soc. 29 (2008) 2399–2402.

[56] M.S. Lah, M.M. Dixon, K.A. Pattridge, W.C. Stallings, J.A. Fee, M.L. Ludwig, Structure-function in *Escherichia coli* iron superoxide dismutase: comparisons with the manganese enzyme from *Thermus thermophilus*, Biochemistry 34 (1995) 1646–1660.

[57] P. Liu, H.E. Ewis, Y.J. Huang, C.D. Lu, P.C. Tai, I.T. Weber, Structure of *Bacillus subtilis* superoxide dismutase, Acta Crystallogr. Sect. F: Struct. Biol. Cryst. Commun. 63 (2007) 1003–1007.

[58] U.G. Wagner, K.A. Pattridge, M.L. Ludwig, W.C. Stallings, M.M. Werber, C. Oefner, F. Frolow, J.L. Sussman, Comparison of the crystal structures of genetically engineered human manganese superoxide dismutase and manganese superoxide dismutase from *Thermus thermophilus*: differences in dimer–dimer interaction, Protein Sci. 2 (1993) 814–825.